Available online at www.sciencedirect.com
ScienceDirect
Acta Biomaterialia 5 (2009) 2258–2269
Acta BIOMATERIALIA
www.elsevier.com/locate/actabiomat

Enhanced osseointegration of grit-blasted, NaOH-treated and electrochemically hydroxyapatite-coated Ti–6Al–4V implants in rabbits

Dror Lakstein [a,b], William Kopelovitch [a], Zahava Barkay [c], Medlej Bahaa [d], David Hendel [b], Noam Eliaz [a,*]

[a] *Biomaterials and Corrosion Laboratory, School of Mechanical Engineering, Tel-Aviv University, Ramat Aviv, Tel-Aviv 69978, Israel*
[b] *Department of Orthopaedic Surgery, Edith Wolfson Medical Center, Holon 58100, Israel*
[c] *The Wolfson Applied Materials Research Centre, Tel-Aviv University, Ramat Aviv, Tel-Aviv 69978, Israel*
[d] *Department of Anatomy and Anthropology, Sackler Faculty of Medicine, Tel-Aviv University, Ramat Aviv, Tel-Aviv 69978, Israel*

Received 25 November 2008; received in revised form 8 January 2009; accepted 26 January 2009
Available online 3 February 2009

Abstract

Osseointegration, in terms of the bone apposition ratio (BAR) and the new bone area (NBA), was measured by backscattered electron imaging. The results were compared for four implant types: grit-blasted and NaOH-treated Ti–6Al–4 V (Uncoated-NaOH), electrodeposited with hydroxyapatite without alkali treatment (ED-HAp), electrodeposited with hydroxyapatite after alkali treatment (NaOH-ED-HAp), and plasma sprayed with hydroxyapatite (PS-HAp). No heat treatment was done after soaking in NaOH. The implants were press fitted into the intramedullary canal of mature New Zealand white rabbits and analyzed, both at the diaphyseal and at the metaphyseal zones, either 1 week or 12 weeks after surgery. NaOH-ED-HAp already exhibited a higher BAR value than the ED-HAp at 1 week, and was as good as the commercial PS-HAp at 12 weeks. The NBA value for NaOH-ED-HAp at 12 weeks was the highest. The higher content of octacalcium phosphate in NaOH-ED-HAp, as evident from the X-ray photoelectron spectroscopy analysis of the oxygen shake-up peaks, and the associated increase in the solubility of this coating in vivo are considered responsible for the enhanced osseointegration. Taking into account also the reduced occurrence of delamination and the inherent advantages of the electrodeposition process, electrodeposition of HAp following soaking in NaOH may become an attractive alternative for the traditional plasma-sprayed process for coating of orthopedic and dental implants.

Keywords: Hydroxyapatite coating; Electrochemistry; Plasma spraying; Osseointegration; In vivo test

1. Introduction

A key factor for the successful fixation of cementless implants used for joint reconstruction is the establishment of a stable interface between the implant and bone. Coating of the implant with osteoconductive hydroxyapatite (HAp, $Ca_5(PO_4)_3(OH)$) is a well-known method for achieving such fixation [1]. It has been shown that, for consistent performance, HAp coatings should have a proper value of porosity, high cohesive strength, good adhesion to the substrate, moderate to high crystallinity, and high chemical and phase stability [2].

HAp-related bone formation is believed to begin with surface dissolution of the HAp, which releases calcium and phosphate ions into the space around the implant. Reprecipitation of carbonated apatite then occurs on the coating surface [3]. The HAp binds serum proteins and cellular integrin receptors, allowing osteoblastic cells to bind to the surface [4,5]. Bone formation follows at both the bone and the coating surfaces [6]. Bone ongrowth develops more rapidly on coatings with low crystallinity because the

* Corresponding author. Tel.: +972 3 6407384; fax: +972 3 6407617.
E-mail address: neliaz@eng.tau.ac.il (N. Eliaz).

1742-7061/$ - see front matter © 2009 Acta Materialia Inc. Published by Elsevier Ltd. All rights reserved.
doi:10.1016/j.actbio.2009.01.033

initial dissolution and release of calcium ions is faster than those associated with coatings of high crystallinity [5,7]. Surface dissolution is therefore a driving force for bone formation, yet the effect of surface roughness on bone apposition may be more significant. It has been shown that rough surfaces exhibit stronger interfaces with bone than do smooth surfaces, in both humans and animals, as long as the interface is bone ongrowth [8,9].

HAp coatings are applied commercially mainly by the plasma-sprayed (PS) process [6]. Since the 1990s, however, much interest in electrodeposition (ED) has evolved [10–20] due to: (i) the low temperatures involved, which enable formation of highly crystalline deposits with low solubility in body fluids and low residual stresses; (ii) the ability to coat porous, geometrically complex or non-line-of-sight surfaces; (iii) the possible improvement of the substrate/coating bond strength; (iv) the ability to control the thickness, composition and microstructure of the deposit; and (v) the ability to incorporate biological matter in the coating during its processing.

Wang et al. [16] studied the osseointegration of uncoated, PS-HAp-coated and ED-HAp-coated Ti–6Al–4V in a canine trabecular bone at 6 h, 7 days and 14 days post-implantation. The PS-HAp was found to provide higher bone apposition ratio than those exhibited by the bare alloy and ED-HAp at 7 days post-surgery. However, at 14 days post-surgery the ED-HAp and PS-HAp coatings exhibited similar bone apposition ratios, much higher than that of the uncoated alloy. This behavior was explained in terms of the lower crystallinity, and consequently higher solubility, of the PS coating compared to the ED coating.

Two shortcomings of the study described in Ref. [16] are: (i) the poor adhesion of the ED-HAp to the metal substrate due to the absence of surface pretreatment; and (ii) the relatively short times of implantation. The objective of the present investigation was to overcome these shortcomings whilst providing insights on the combined effects of grit blasting and soaking in NaOH before electrochemical deposition of HAp.

Grit blasting was applied to either improve the osseointegration of the uncoated implants or increase the adhesion of the ED-HAp coating to the Ti–6Al–4V substrate. Several benefits of this treatment have already been demonstrated elsewhere [21–24].

Soaking of titanium and its alloys in aqueous solution of 5 M NaOH at 60 °C for 24 h and subsequent heat treatment (usually, at 600 °C for 1 h) has been found to form a bioactive surface that spontaneously induces nucleation of bone-like apatite in vivo [25–30]. Similarly, it was hypothesized that this process would lead to enhanced nucleation of the synthetic ED-HAp coating, resulting in increased coating/substrate adhesion strength.

Although most studies have applied heat treatment, and sometimes even found it mandatory in order to achieve good performance [27], it was decided to omit this stage in the present study because such treatment might result in degradation of the mechanical properties of the metal substrate. Regarding the implantation period, it has been argued that healing periods longer than 4 weeks do not further increase the quantity of bone ingrowth into implants with porous surfaces [31]. On the other hand, while HAp-coated implants inserted into cortical bone have been reported to achieve their maximum bone apposition 4 weeks post-implantation, uncoated surfaces were found to increase their bone apposition ratios until 12 weeks [32]. Hacking et al. [33] also argued that 12-week implantation has a clinical value. Therefore, the selection of this implantation period in the present work should allow for complete osseointegration of both coated and uncoated implants, thereby allowing for precise comparative study.

2. Materials and methods

2.1. Implant preparation

A Ti–6Al–4V ELI grade rod (ASTM F136-02a) rod, 4.76 mm in diameter, was produced by Dynamet, Inc. (Washington, PA) and supplied by Barmil (Petach-Tikva, Israel). This rod was machined into 25-mm-long sample rods that were subsequently cleaned with paper and MEK, then ultrasonically in acetone. Twelve rods were plasma sprayed with 80-μm-thick HAp. This group will be termed hereafter PS-HAp. Thirty-six rods were chemically etched in HF/HNO_3 solution for 2 min, washed with DI water, dried and then grit-blasted (GB) with high-purity (98.2%) white alumina powder from Calbex Mineral Trading, Inc. (Henan, China). The blasting parameters were: grit size of F200–F180 (59–68 μm), pressure of approximately 6 atm and working distance of about 10 cm. Blasting with alumina powder was preferred over blasting with silica powder because of biocompatibility aspects. After grit blasting, the rods were cleaned ultrasonically. Twelve of these rods were subsequently electrodeposited with HAp; these will hereafter be referred to as ED-HAp. The remaining 24 rods were soaked in a stirred solution of 5 M NaOH at 60 °C for approximately 14 h. Afterwards, they were cleaned ultrasonically in acetone and then in ethanol, washed with Millipore water (Milli-DI™, Millipore Corporation, Billerica, MA), dried and then kept in a clean environment. Complementary heat treatment was not applied. Of these rods, 12 were left uncoated; these will hereafter be referred to as Uncoated-NaOH. The last 12 rods were subsequently electrodeposited with HAp; these will hereafter be referred to as NaOH-ED-HAp.

Electrodeposition was carried out in a standard three-electrode cell in which two graphite rods were used as the auxiliary electrode, a saturated calomel electrode (SCE) was used as the reference electrode and the sample rod was used as the working electrode. The electrolyte was prepared by dissolving 0.61 mM $Ca(NO_3)_2$ and 0.36 mM $NH_4H_2PO_4$, both AR-grade from Merck (Darmstadt, Germany), in Millipore water. The acidity was measured using an InoLab pH/Oxi Level 3 meter (WTW GmbH, Weilheim, Germany) and adjusted to pH 6.0 so that the electro-

lyte was saturated with calcium and phosphate ions. No nitrogen purging was carried out during deposition. A Lauda Gmbh (Lauda Königshofen, Germany) Ecoline model E-220T thermostatic bath was used to maintain a constant temperature of 84 ± 1 °C. Stirring at 200 rpm was maintained by means of a Maxi S flat magnetic stirrer with Telemodul 40S controller from H+P Labotechnik AG (Oberschleissheim, Germany). An EG&G/PAR (Princeton, NJ) model 263A potentiostat/galvanostat operating in potentiostatic mode was employed to maintain the cathode potential at −1.4 V vs. SCE for 2 h. Following electrodeposition, the implants were washed in DI water, rinsed in warm DI water for about 10 min, dried and stored in polyethylene bags separately. All implants were vacuum bagged and sterilized by gamma irradiation at Sor-Van Radiation, Ltd. (Kiriat Soreq, Israel). They were exposed to a dose of 30 kGy (3.0 Mrad). Gamma irradiation was preferred over ethylene oxide gas because the latter might lead to coating detachment and requires a long rest time for degassing. Thus, the data constructed in this study is comparable to the actual solution on the market.

2.2. Surface characterization of non-implanted rod samples

A representative group of implants was examined in an environmental scanning electron microscope (ESEM) in the pre-implanted, sterilized condition. The goal was to document the characteristic surface morphology and chemical composition of each type of implant. Features such as coating uniformity and presence/absence of cracks were also sought.

X-ray photoelectron spectroscopy (XPS) measurements and analysis were performed in accordance with the procedure described elsewhere in detail [18]. The atomic ratios Ca/P and O/Ca were determined from high-resolution spectra. In order to identify unambiguously the specific CaP formed, the integrated intensity of the oxygen shake-up peaks [34] was calculated.

2.3. Surgical procedure

The animal protocols were approved by the Institutional Animal Care and Use Committee (IACUC) of the Sackler Faculty of Medicine at Tel-Aviv University. The sample rods were implanted in 14 mature New Zealand white rabbits that were obtained from Harlan Laboratories, Ltd. (Rehovot, Israel). The animals weighed between 3.0 and 4.0 kg (mean 3.57 kg). The rabbits randomly received two different implants, one in each distal femur. The animals were anesthetized with intramuscular injections of 40 mg kg^{-1} ketamine and 5 mg kg^{-1} xylazin hydrochloride, and were administered a single 80 mg dose of Cefazolin IV. Under sterile conditions, a medial parapatellar arthrotomy was performed. A 2-mm Kirschner wire was inserted through the distal femur and into the intramedullary canal. This canal was then hand reamed with 2.7, 3.5, 4.0, 4.5 and 4.8-mm drill bits (Fig. 1). The implants were press fitted into the medullary canal until they were flush with the articular surface. The distal portion of the implant was within the metaphysis, while the proximal portion was within the diaphysis (Fig. 2). There were neither restric-

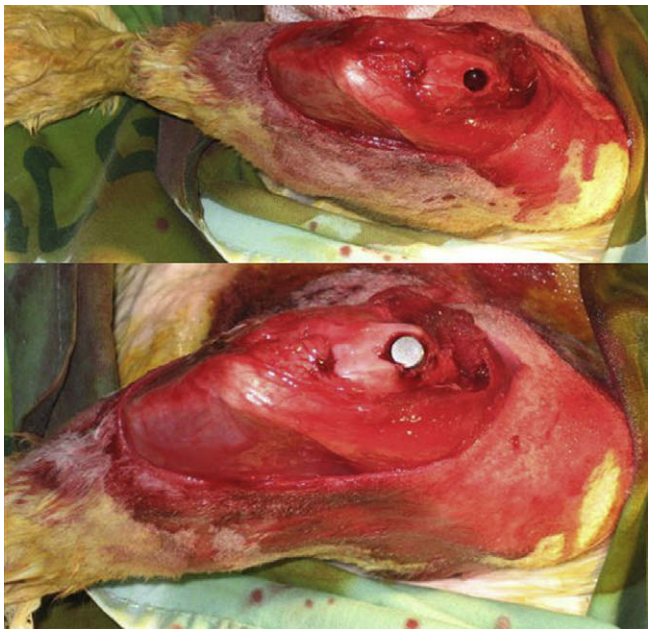

Fig. 1. A widened hole in the medullary canal of the distal femur of the rabbit before (top) and after (bottom) press fitting of the implant.

Fig. 2. Radiographs of the right distal femur of a rabbit (bottom, LAT; top, AP). The implant is press fitted into the medullar canal, within both the metaphysis and diaphysis.

tions on walking after the surgeries nor cases of postoperative infections or other complications in the analyzed rabbits. In addition to the 14 analyzed rabbits, one rabbit died during the procedure and three rabbits had early postoperative fractures. It should be emphasized that this non-weight-bearing intramedullary implant model is different from the weight-bearing transcortical model; the former better simulates the clinical implant site than does the latter [22,35].

2.4. Histological examination

Two groups, one of four rabbits and one of 10 rabbits, were sacrificed after 1 week and 12 weeks of implantation, respectively. The rabbits were killed with a lethal intravenous dose of pentobarbital. The distal femora were removed and stripped out of soft tissue. The specimens were fixated in buffered formalin for 7 days. After rinsing in water, the samples were dehydrated in ascending concentrations of ethanol (70%, 83%, 96% and twice 100%), approximately 24 h in each. After dehydration, samples were fixated in xylene for 1 day, then embedded in a mixture of 100 cm^3 of methyl methacrylate, 10 cm^3 of polyethylene glycol and 1 g of benzoyl peroxide at room temperature. Thus, after approximately 2 weeks a rigid piece of a sample embedded in PMMA was formed. Next, two 200-μm-thick cross-sectional slices, one from the diaphysis and one from the metaphysis, were cut using a water-cooled low-speed diamond precision saw (Isomet from Buehler, IL). The slices were glued, using acrylic glue, onto support Perspex "milky" slides, then ground and polished on a precision grinder (Buehler, IL) down to a thickness of 20 μm. These slides were stained with either toluidine blue or hematoxylin and eosin after immersion in formic acid and inspected under Olympus (Nagano, Japan) IX71 light microscope. Cross-sections were also ground down to P1000 and analyzed in a Quanta 200 FEG ESEM from FEI (Eindhoven, The Netherlands) in low-vacuum mode in order to avoid charging of the constitute materials.

Both the bone apposition ratio (BAR; also known as the apposition index, AI) [16,21,36] and the new bone area (NBA) [22,37,38] were measured as indicators of osseointegration. Backscattered electron (BSE) images in the SEM provide high contrast for differentiating between the various components, which was found to be most useful for these measurements. The attached Oxford Si EDS detector was further used to distinguish between the alloy substrate, the HAp coating and bone via element composition. The BAR represents the length of the direct implant surface/bone contact divided by the length of the outer circumference of the implant. Its measurement consisted of four steps. First, BSE images were recorded around the periphery of each implant at a magnification of 150×. For each implant, approximately 20 such images were collected and stored in digital format (1024 × 884 bytes). The images were merged into a single image, which showed the whole circumference of the implant. Secondly, a grid was superimposed on the image. This grid was pixel-calibrated, forming 50 μm × 50 μm squares. Thirdly, manual determination of positive/negative bone apposition was done in each square, which was colored accordingly. Finally, automatic pixel counting was applied. Thus, the BAR was calculated through division of the positive pixels count by the sum of the positive and negative counts. The NBA represents the percentage of new bone within a distance of either 0.5 or 1 mm from the implant surface at the diaphysis and metaphysis, respectively. In order to calculate it, rings were created, with the implant perimeter being the inner surface of the ring. The sum of pixels that represented new bone was calculated and divided by the total number of pixels inside the ring.

2.5. Statistical analysis

The primary endpoint study, after the 12-week implantation, consisted of four different types of implant, each being implanted in five rabbits. The secondary endpoint study, after 1-week implantation, consisted of smaller, varying sample sizes of the four types. The appropriate sample size n for the 12-week study was designed so as to achieve a power of 80% using a significance level $\alpha = 0.05$ in a two-sided test when the absolute value of the distance between the means of the BAR for the uncoated vs. coated samples is 10%. Thus, a requirement for five implanted samples from each of the four types was pre-defined.

The BAR and NBA values are reported as mean ± standard deviation. A one-way analysis of variance (ANOVA) and Tukey post hoc (multiple comparisons) test were applied using the SPSS statistical package. Differences of $p < 0.05$ are considered to be statistically significant.

3. Results

3.1. Surface morphology and chemistry of non-implanted rods

Fig. 3 shows the typical surface morphology of each type of implant in the sterilized condition, prior to implantation, at low (left) and high (right) magnifications. Fig. 3a demonstrates the plastic deformation of the surface due to GB. The needle-like morphology of calcium phosphate (CaP) is evident in Fig. 3b and c. Further analysis revealed that these needles were actually prismatic hexagonal bars, approximately 300 nm in diameter, that represented single crystals. Single crystals of natural HAp have also been reported to have hexagonal space group $P6_3/m$ [39]. The needles are arranged in clusters with varying orientations that are probably related to the walls of the microcraters formed by GB. The morphology suggests that the coating is fairly crystalline. No significant difference was observed between NaOH-ED-HAp and ED-HAp. The ED coatings were found to cover the surface uniformly and contained no evident cracks. The PS-HAp (Fig. 3d) demonstrates a

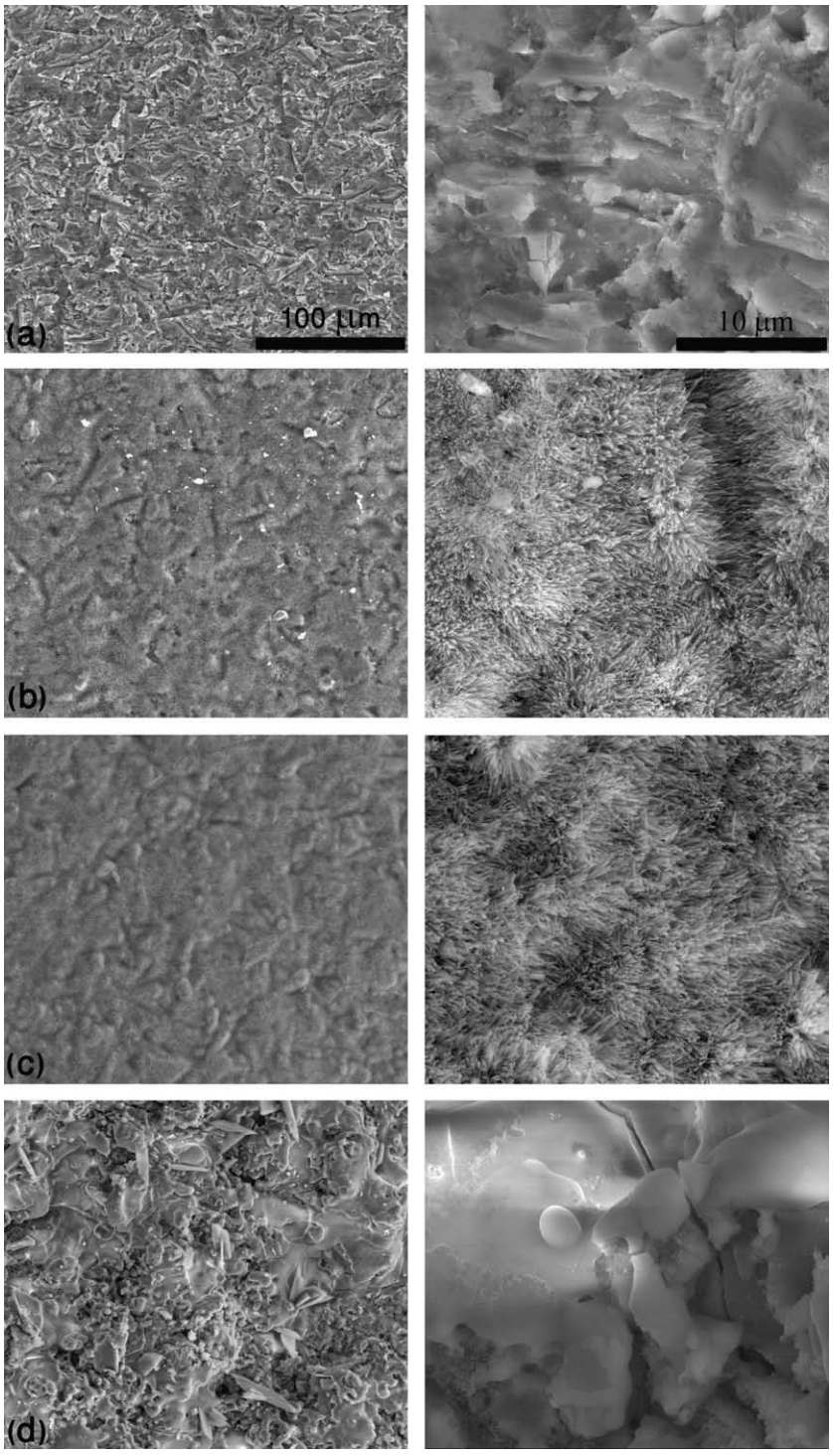

Fig. 3. Representative ESEM images of sterilized implants before implantation. Low- and high-magnification images are provided for each implant, on the left and right side, respectively. (a) Uncoated-NaOH, (b) ED-HAp, (c) NaOH-ED-HAp and (d) PS-HAp.

significantly different surface morphology – large globules (solidified molten splats) with no resolved HAp crystallites – and is much denser than the ED coatings. Some cracking was found on the surface of the PS coating.

Low-resolution XPS survey spectra revealed Ti, Al and V from the alloy, O from the oxide layer and Ar from the sputter cleaning medium at the surface of Uncoated-NaOH; Ca, P and O from CaP and C from carbonate contamination at the surface of ED-HAp; Ca, P and O from CaP, C and N due to adsorption from the outer atmosphere, and Zn impurity at the surface of NaOH-ED-HAp; and Ca, P and O from CaP as well as C, Na and Mg impurities at the surface of PS-HAp. The atomic concentrations of elements obtained from high-resolution

Table 1
Chemical composition (at.%) of the uncoated and CaP-coated Ti–6Al–4V samples, as determined by low- (uncoated sample) and high- (all coated samples) resolution XPS scans.

Element	Uncoated-NaOH	ED-HAp	NaOH-ED-HAp	PS-HAp
O	53.79	50.85	36.86	55.28
Ca	0.14	15.73	15.38	17.15
P	–	11.57	10.56	15.18
C	3.77	21.85	37.20	12.39
Ti	14.10	–	–	–
Al	27.61	–	–	–
V	0.59	–	–	–
Ca/P	N/A	1.36	1.46	1.13
O/Ca	N/A	3.23	2.40	3.22
$O(1s)_{II}/O(1s)$	N/A	0.0585	0.0563	0.0586

XPS measurements are given in Table 1, together with the Ca/P and O/Ca atomic ratios. In comparison, the theoretical Ca/P ratios are 1.00, 1.33, 1.50, 1.50 and 1.67 for dibasic calcium phosphate anhydrous (DCPD, brushite), octacalcium phosphate (OCP), amorphous calcium phosphate (ACP), tricalcium phosphate (TCP) and HAp, respectively. The theoretical O/Ca ratios are 6.00, 3.125, 3.00, 2.67 and 2.60 for these phases, respectively. The measured Ca/P and O/Ca ratios for ED-HAp fit best the theoretical values for OCP. The measured Ca/P and O/Ca ratios for NaOH-ED-HAp fit best the theoretical values for either TCP or HAp. The measured Ca/P and O/Ca ratios for PS-HAp may indicate some mixture of DCPD and OCP. However, it should be noted that the measured Ca/P atomic ratio, obtained from conventional XPS analysis, has been found to be always lower than the theoretical value for different calcium phosphates on the surface, thus preventing their unambiguous identification [34]. Therefore, in order to identify the phases in a more definite way, the oxygen loss spectrum was analyzed. The values of $O(1s)_{II}/O(1s)$ are provided in Table 1. In comparison, Lu et al. [34] measured mean $O(1s)_{II}/O(1s)$ ratios of 0.072, 0.065, 0.053, 0.037, 0.020 and 0.008 for powders of TCP, HAp, OCP, dibasic calcium phosphate anhydrous, DCPD and monobasic calcium phosphate monohydrate, respectively. Thus, the measured values reported in Table 1 all fall between the values previously reported as typical of OCP and HAp. This finding is supported by a previous study, in which OCP was observed as a precursor to HAp [18]. The NaOH-ED-HAp sample exhibits an $O(1s)_{II}/O(1s)$ value slightly lower than that for the other two types of coated samples, and somehow closer to the value for OCP. Combining the shake-up peaks analysis with the measured Ca/P and O/Ca values, it seems with a high level of certainty that both types of ED-HAp consist of both OCP and HAp, the content of the former being possibly higher in the NaOH-ED-HAp sample. It should be noted that ACP and OCP have been observed in vitro to be deposited before HAp on NaOH-treated titanium surfaces [40]. The PS-HAp sample seems to consist of a mixture of several phases, presumably OCP, DCPD and HAp. The presence of several phases was supported by ESEM/EDS observations.

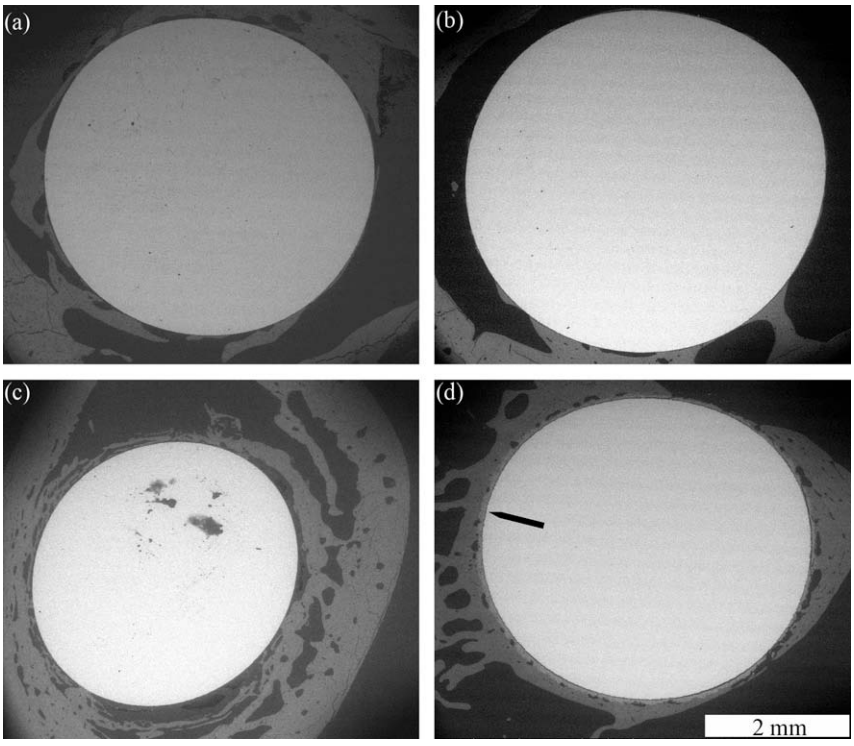

Fig. 4. ESEM images of the bone/implant interface zone at low magnification after 12-week implantation. (a) Uncoated-NaOH, (b) ED-HAp, (c) NaOH-ED-HAp (d) PS-HAp. The arrow in (d) indicates on the PS coating layer.

3.2. Microscopic evaluation of the bone/implant interface

Fig. 4 shows the bone/implant interface zone at low magnification after the 12-week implantation. Both the ED-HAp and the NaOH-ED-HAp coatings are relatively thin (~5 μm) and cannot be easily identified at this magnification. The PS-HAp coating, on the other hand, is much thicker (up to 90 μm thick) and can thus be identified (indicated by arrow).

Figs. 5 and 6 demonstrate typical BSE-ESEM images of the four types of implants after the 1- and 12-week implantation, respectively. At 12 weeks, much more new bone is evident in contact with the implant, conforming to its surface more closely. The adjacent bone is characterized by clearly defined osteons and remnants of interstitial bone. The presence of many Haversian canals as well as numerous osteocytic lacunae and canaliculi in the bone adjacent to the surface of the implant indicates that the implanted biomaterial was well tolerated. No intervening fibrous tissue was seen. Cracking in the surrounding bone, as seen in Fig. 6, has been observed by others too [16,21,35,38].

In some regions on the surface of the PS-HAp-coated samples, the coating was missing and bone could be seen apposing directly the titanium surface. Because delamination of commercial PS-HAp coatings is one of the major technological concerns, careful microscopic examination of all interfaces was made. It was found that the PS-HAp coating had a higher tendency to delaminate compared to either the ED-HAp or the NaOH-ED-HAp coating. At low magnifications, where macroscopic delamination can be noticed, this higher tendency was reflected by a three times higher number of occurrences of delamination in PS-HAp implants. At high magnifications, where microscopic delamination can be noticed, the difference was even more significant, with all PS-HAp implants exhibiting some delamination, at both the diaphysis and metaphysis zones.

Fig. 7 presents typical light microscope images of histological sections after the 12-week implantation. New bone is clearly evident around all four types of implant.

3.3. BAR measurements

One week post-surgery, only eight implants (four rabbits) were evaluated altogether. The mean BAR values are given in Table 2. Although these data have no statistical significance, it seems that the NaOH-ED-HAp and PS-HAp implant types do have higher osseointegration at this early stage of implantation.

Twelve weeks post-surgery, significant increase in the BAR was observed for all four types, as evident in Fig. 8. ANOVA yielded $p = 0.104$ (i.e. $p > 0.05$) for the diaphysis, meaning that there was no significant difference between the groups. For the metaphysis, however, $p = 0.005$ was obtained, indicating that there was significant difference between the groups. Thus, the Tukey post hoc test was applied to the metaphysis only. It was found that the only groups with a significant difference between each other were Uncoated-NaOH and ED-HAp ($p = 0.027$), Uncoated-

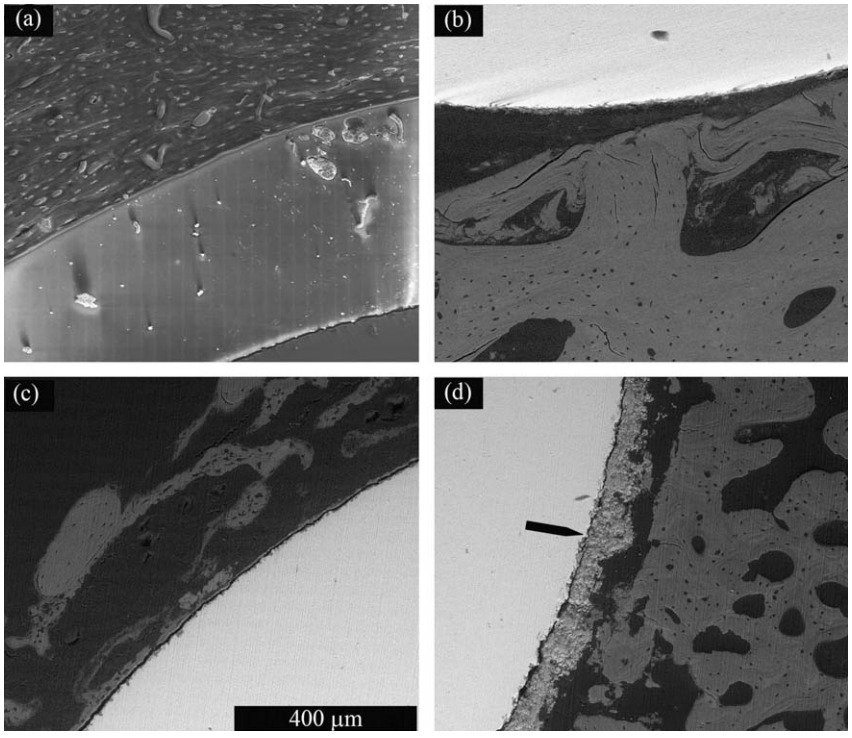

Fig. 5. ESEM images of the bone-implant interface at 1 week. (a) Uncoated-NaOH, (b) ED-HAp, (c) NaOH-ED-HAp and (d) PS-HAp. Images (c) and (d) represent the metaphyses of the left leg and right leg, respectively, of the same rabbit. The arrow in (d) indicates on the PS coating layer.

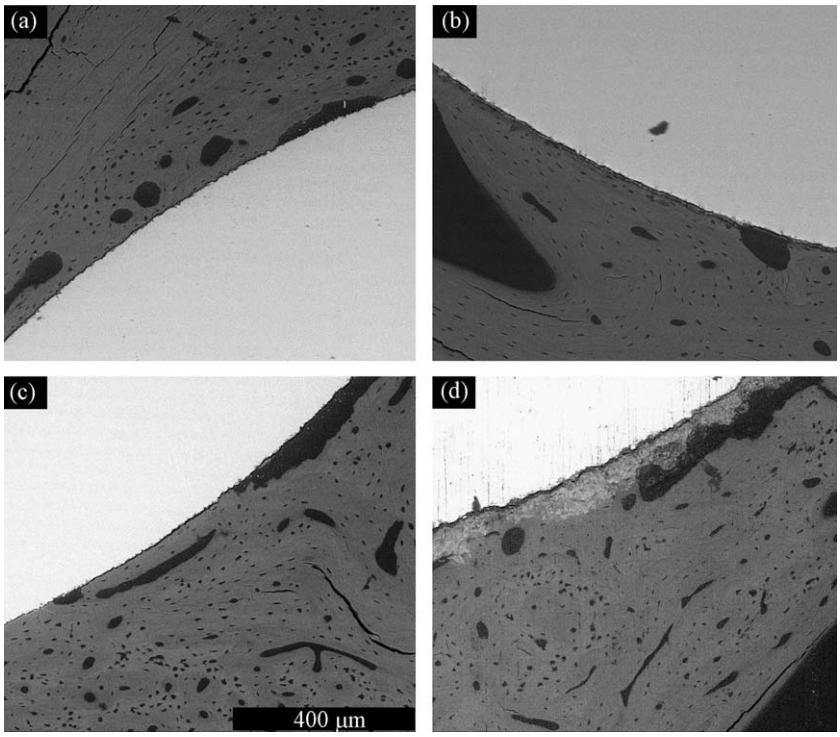

Fig. 6. ESEM images of the bone-implant interface at 12 weeks. (a) Uncoated-NaOH, (b) ED-HAp, (c) NaOH-ED-HAp and (d) PS-HAp. Images (a) and (b) represent the diaphyses of the right and left leg, respectively, of the same rabbit.

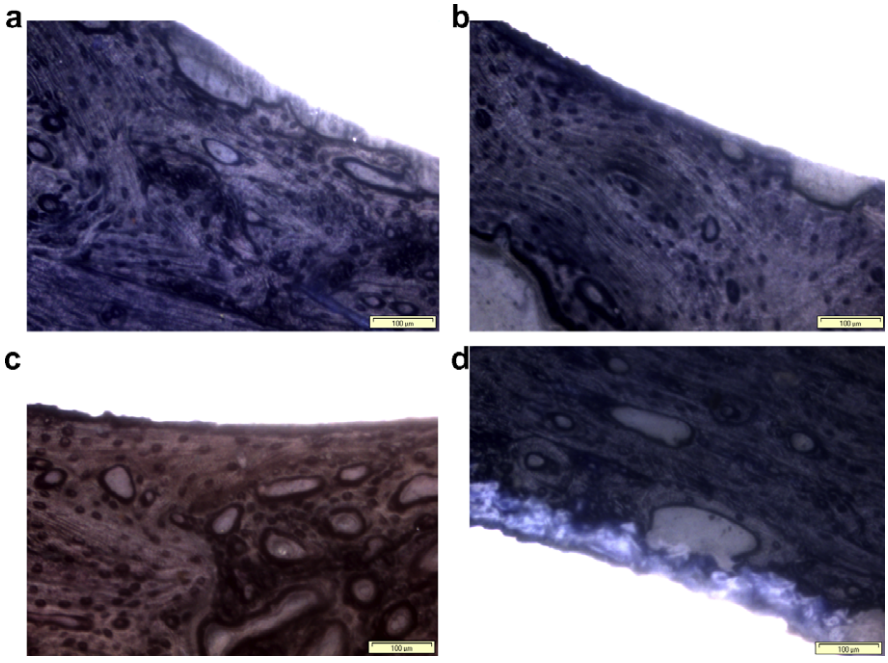

Fig. 7. Light microscope images of histological samples after 12-weeks implantation. (a) Uncoated-NaOH, (b) ED-HAp, (c) NaOH-ED-HAp and (d) PS-HAp. Each scale bar equals 100 μm.

Table 2
Bone apposition ratio (BAR) values for different implant types at 1 week post-implantation.

Implantation site	Uncoated-NaOH (%)	ED-HAp (%)	NaOH-ED-HAp (%)	PS-HAp (%)
Metaphysis	4.2	1.8	17.9	16.5
Diaphysis	2.5	5.7	18.2	12.8

NaOH and NaOH-ED-HAp ($p = 0.004$), and Uncoated-NaOH and PS-HAp ($p = 0.046$).

3.4. NBA measurements

In contrast to the BAR measure, the NBA provides information on the new bone growth in vicinity to the

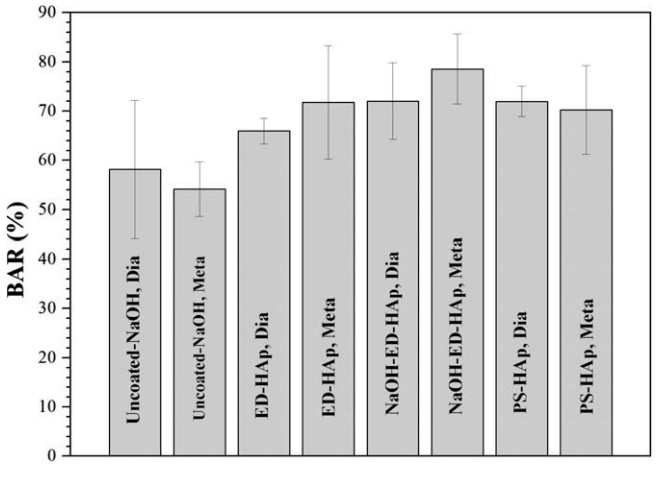

Fig. 8. Bone apposition ratio (BAR) values 12 weeks post-surgery, at both the diaphysis and metaphysis.

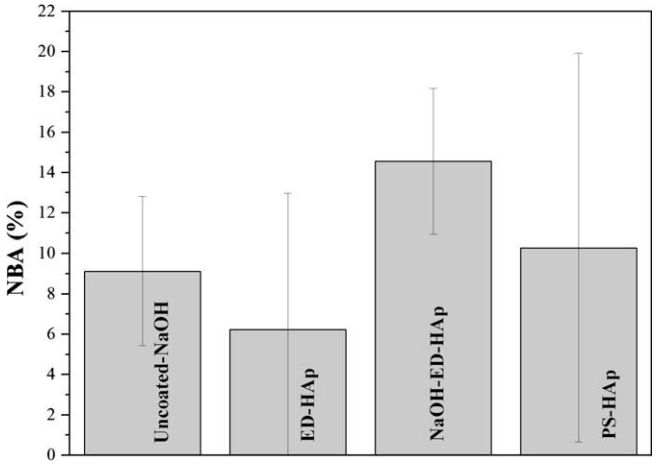

Fig. 9. New bone area (NBA) values at the metaphysis, 12 weeks post-surgery.

implant, but not necessarily in direct contact with its circumference. Twelve weeks post-surgery, the NBA values illustrated in Fig. 9 were measured for the metaphysis. ANOVA yielded $p = 0.301$ (i.e. $p > 0.05$), meaning that there was no significant difference between the four groups. However, the NaOH treatment seems to be beneficial, resulting in the highest mean NBA value for NaOH-ED-HAp, and in high NBA value of Uncoated-NaOH compared to ED-HAp.

4. Discussion

The histomorphometric measurements in this study were done on SEM-BSE images, which have been claimed to provide more accurate quantitative analysis compared to either light microscope images of stained samples or micro-radiographic images [35,41]. The increase in the BAR values from 1 week to 12 weeks after implantation is evident in all four implant groups, either at the metaphysis or at the diaphysis. The BAR values measured at 12 weeks are somewhat high compared to those reported in some previous studies for the same implantation period in the medullary canal of rabbit femora [22,38]. Other values are available for implant in canine femoral medullary canal [35,42]. The in vivo performance of the ED implants may also be appreciated when comparing to the work of Schmidmaier et al. [43], in which BAR values of 26 ± 18 and $68 \pm 21\%$ were measured for uncoated sand-blasted Ti and functionally graded ED-HAp implants, respectively, implanted in rats for 24 weeks.

NBA measurements are less common in the literature than BAR measurements, possibly because the former might be more complicated to do accurately. For the same samples, the NBA values are lower than the respective BAR values, as anticipated. Comparison can be made to NBA values reported elsewhere [37,38].

Comparison is made in this study between the osseointegration at the diaphyseal and metaphyseal zones. Twelve weeks post-surgery, the difference between the BAR values for the four groups was more pronounced at the metaphysis, compared to the diaphysis. It should be noted that, at the diaphysis, native bone is in close contact with the implant. The metaphysis, on the other hand, contains cancellous bone and is more reactive (e.g. it usually provides faster facture healing). In addition, the results in this study reflect biological bone growth per se, as no load transfer exists. Jinno et al. [22] found that the BAR decreased from the diaphysis to the proximal metaphysis, and from there to the distal metaphysis. Feighan et al. [21], on the other hand, reported a similar trend for the osseointegration at the diaphysis and at the proximal part of the metaphysis.

It has been mentioned that one of the shortcomings that had been observed in the work of Wang et al. [16], which the present work was expected to overcome, is poor adhesion of the ED-HAp coating to the substrate when the surface is not prepared properly. Thus, chemical etching in HF/HNO_3, grit blasting and soaking in NaOH were applied in the present work. Consequently, both the ED-HAp and the NaOH-ED-HAp coatings revealed lower tendency to delaminate compared to the commercial PS-HAp coating. The beneficial effect of these surface pretreatments is supported also by in vitro mechanical tests (to be published), in which the addition of a GB-NaOH combination to samples ground at P1000 and subsequently etched in HF/HNO_3 resulted in an increase in the adhesion strength, from 17.1 to 28.5 MPa. In certain cases, the mode of failure actually changed from pure adhesive to combined adhesive–cohesive. The reason for the higher tendency to delaminate of the PS-HAp coating is most likely the combination of thicker PS coatings and residual thermal stresses that were incorporated during the PS process. The origin of the latter is the mismatch in the thermal expansion coefficients of the ceramic coating and the metal substrate. In the present in vivo study, cracking occurred either within the coating layer or at the metal/coating interface,

but not at the coating/bone interface. This observation is in accordance with previous reports that the coating/bone interface is stronger than either the coating itself or its bonding to the substrate [44].

Two of the major factors that affect the osseointegration and the interfacial strength between an implant and bone are the surface chemistry and roughness. These two factors varied among the four groups of implants analyzed in the present study (see Section 3.1). But which of the two factors is more important with respect to HAp coatings? Hacking et al. [42] referred to this question, using a canine femoral intramedullary implant model. Grit-blasted CP–Ti implants were compared to HAp-coated implants, as well as to implants first coated with HAp and then recoated with a very thin titanium film that preserved the topography of the HAp coating but masked the chemistry of HAp. Twelve weeks after implantation, bone apposition averaged 23% for the GB-CP-Ti implants, 73.6% for the HAp-coated implants and 59.1% for the HAp-Ti-coated implants. The interfacial strength of the recoated implants was about 80% of that achieved when HAp was exposed. Thus, the investigators argued that surface roughness was a larger contributor to interface strength than was the presence of the HAp chemistry. However, it should be borne in mind that while surface roughness is undoubtedly a factor in determining the interfacial strength when an implant is in intimate contact with bone, implants are often surrounded by gaps, so that micromotion occurs after implantation. Under these circumstances, the osteoconductive nature of the HAp coating is probably a key factor in promoting the intimate bone apposition required for the achievement of interface stability.

The major finding in this investigation is that soaking the Ti–6Al–4V in aqueous solution of NaOH without complementary heat treatment accelerated the osseointegration of the ED-HAp coating, as reflected by the BAR value, 1 week after implantation and kept it at least as good as the commercial PS-HAp coating at 12 weeks after surgery. Combining this biological behavior with the reduced coating detachment and the inherent advantages of the electrodeposition process, it is evident that the combination of mechanical (GB) and chemical (soaking in NaOH) pretreatments and electrodeposition of HAp provides a system that may become preferable to the traditional plasma spraying process for the coating of orthopedic and dental implants. The exclusion of heat treatment after soaking in NaOH makes it even more attractive, both industrially and clinically. As the surface morphologies (ESEM data) of the NaOH-ED-HAp or the ED-HAp were similar, it may be speculated that the higher content of the OCP phase in the NaOH-ED-HAp coating and the associated increase in the solubility of this coating in vivo are responsible for the enhanced osseointegration. Various chemical, biological and mechanical effects of soaking titanium and its alloys in NaOH, before and after the complementary heat treatment, have been discussed elsewhere in detail [25–30,40,45]. Kokubo et al. [25] suggested that when titanium is soaked in an NaOH solution, a hydrated titanium oxide gel layer containing Na^+ ions is formed on the surface. Because this gel layer contains a considerable amount of water or hydrated ions, it is mechanically unstable. Thus, the role of the complementary heat treatment is to dehydrate and densify this gel layer, forming an amorphous sodium titanate layer with a porous network structure, which is tightly bonded to the metal substrate. When the alkali- and heat-treated titanium is exposed to simulated body fluid (SBF), Na^+ ions are released from the amorphous layer while H_3O^+ cations are incorporated in the surface layer, resulting in the formation of Ti–OH groups on the surface. The released alkali cations also increase the degree of supersaturation with respect to apatite, by increasing the local pH. Electrostatic interaction between the negatively charged units of titania, which are dissociated from the Ti–OH groups, and the positively charged calcium ions in the fluid results in the formation of amorphous calcium titanate. The amorphous calcium titanate, which is hypothesized to have a positive charge, attracts phosphate ions from the surrounding fluid, forming amorphous calcium phosphate, which is then converted to the crystalline HAp [28].

Nishiguchi et al. [29] evaluated the effect of NaOH treatment on CP-Ti implanted in the medullary canal of rabbit distal femora. After 12 weeks of implantation, they measured BAR values of $55.8 \pm 6.0\%$ and $19.2 \pm 10.3\%$ for NaOH-treated and untreated (ground) titanium, respectively. This value for the NaOH-treated implant is similar to the one measured in the present work for grit-blasted and NaOH-treated, uncoated Ti–6Al–4V alloy, but is much higher than typical values reported in the literature for uncoated titanium implants that had not been treated with NaOH. It should be noted that while, in the present work, GB was applied whereas complementary heat treatment was not, Nishiguchi et al. [29] did not use GB but did apply heat treatment after soaking in NaOH. In another paper [27], Nishiguchi et al. compared the bone-bonding ability of alkali- and heat-treated titanium with that treated in NaOH without subsequent heat treatment. It was concluded that the NaOH-treated titanium without heat treatment had no bone-bonding ability due to its unstable reactive surface layer. The findings in the present work contradict that conclusion. Furthermore, not only does the NaOH soaking per se stimulate the bone ongrowth into the surface of the implant, it also catalyzes biomineralization in the surroundings. Kim et al. [26] previously demonstrated that alkali-treated titanium has a similar ability to form apatite on its surface when exposed to SBF, with or without heat treatment. Park et al. [45] reported that NaOH treatment prior to electrodeposition in a modified SBF resulted in both a denser and more uniform brushite/HAp coating. It was speculated that the porous network of the titanium surface formed after the NaOH pretreatment provided more favorable sites for the nucleation of CaP. It is not certain, however, whether heat treatment was applied in that in vitro study. Hence, this seems

to be the first report in the literature of the beneficial effect of NaOH treatment without complementary heat treatment on both uncoated and electrochemically coated Ti–6Al–4V, both at the diaphysis and at the metaphysis, using a non-weight-bearing intramedullary implant model and a 12-week implantation period, which has a clinical value.

5. Conclusions

In this research, the osseointegration of four implant types was assessed, either 1 week or 12 weeks post-surgery, based on measurements of the bone apposition ratio (BAR) and the new bone area (NBA) at the diaphyseal and metaphyseal zones. The following conclusions were reached:

(1) NaOH-ED-HAp exhibited higher BAR value than the ED-HAp at 1 week, and was at least as good as the commercial PS-HAp both at 1 week and at 12 weeks. At 12 weeks, the difference between the BAR values for the four groups was more pronounced at the metaphysis than at the diaphysis.
(2) The higher content of OCP in NaOH-ED-HAp, as evident from XPS analysis of the oxygen shake-up peaks, and the associated increase in the solubility of this coating in vivo may be responsible for the enhanced osseointegration.
(3) Considering the enhanced biological behavior, the reduced occurrence of delamination and the inherent advantages of the electrodeposition process compared to the plasma spraying process, electrodeposition of HAp following soaking in NaOH may become attractive, both industrially and clinically, for coating cementless implants used for joint reconstruction. The exclusion of heat treatment after soaking in NaOH makes it even more attractive.

Acknowledgments

We thank Mario Levinshtein and Oshrit Ritman from the Biomaterials and Corrosion Laboratory for their technical and statistical analysis work, respectively. We are grateful to Israel Hershkovitz from the Department of Anatomy and Anthropology for letting us use his laboratory facilities and take advantage of his expertise in preparation of histological specimens. The help of Noam Kariv from the Animal House, in both animal care and surgeries, and of Larisa Burstein from the Wolfson Applied Materials Research Centre, in XPS analysis, is appreciated. We express gratitude to Laticia Schreiber from the Edith Wolfson Medical Center and to Victor Goldberg from Case Western Reserve University (OH) for their useful advice regarding histological analysis and surgery, respectively. Finally, we thank the Department of Orthopedics at the Edith Wolfson Medical Center for partially funding this work.

References

[1] Furlong RJ, Osborn JF. Fixation of hip prostheses by hydroxyapatite ceramic coatings. J Bone Joint Surg Br 1991;73:741–5.
[2] Tsui YC, Doyle C, Clyne TW. Plasma sprayed hydroxyapatite coatings on titanium substrate. Part 1, mechanical properties and residual stress levels. Biomaterials 1998;19:2015–29.
[3] LeGeros RZ. Properties of osteoconductive biomaterials: calcium phosphate. Clin Orthop 2002;395:725–33.
[4] Kilpadi KL, Chang PL, Bellis SL. Hydroxyapatite binds more serum proteins, purified integrins, and osteoblast precursor cells than titanium or steel. J Biomed Mater Res 2001;57:258–67.
[5] Porter AE, Hobbs LW, Rosen VB, Spector M. The ultrastructure of the plasma sprayed hydroxyapatite bone interface predisposing to bone bonding. Biomaterials 2002;23:725–33.
[6] Sun L, Berndt CC, Gross KA, Kucuk A. Material fundamentals and clinical performance of plasma-sprayed hydroxyapatite coatings: a review. J Biomed Mater Res B 2001;58:570–92.
[7] Overgaard S, Bromose U, Lind M, Bunger C, Soballe K. The influence of crystallinity of the hydroxyapatite coatings on the fixation of implants. Mechanical and histomorphometric result. J Bone Joint Surg Br 1999;81:725–31.
[8] Wong M, Eulenberger J, Schenk R, Hunziker E. Effect of surface topology on the osseointegration of implant materials in trabecular bone. J Biomed Mater Res 1995;29:1567–75.
[9] Svehia M, Morberg P, Zicat B, Bruce W, Sonnabend D, Walsh WR. Morphometric and mechanical evaluation of titanium implant integration: comparison of five surface structures. J Biomed Mater Res 2000;51:15–22.
[10] Redepenning J, McIsaac JP. Electrocrystallization of brushite coatings on prosthetic alloys. Chem Mater 1990;2:625–7.
[11] Royer P, Rey C. Calcium-phosphate coatings for orthopedic prosthesis. Surf Coat Technol 1991;45:171–7.
[12] Shirkhanzadeh M. Electrochemical preparation of bioactive calcium phosphate coatings on porous substrates by the periodic pulse technique. J Mater Sci Lett 1993;12:16–9.
[13] Vijayaraghavan TV, Bensalem A. Electrodeposition of apatite coating on pure titanium and titanium-alloys. J Mater Sci Lett 1994;13:1782–5.
[14] Shirkhanzadeh M. Direct formation of nanophase hydroxyapatite on cathodically polarized electrodes. J Mater Sci Mater Med 1998;9:67–72.
[15] Eliaz N, Sridhar TM, Kamachi Mudali U, Baldev R. Electrochemical and electrophoretic deposition of hydroxyapatite for orthopaedic applications. Surf Eng 2005;21:238–42.
[16] Wang H, Eliaz N, Xiang Z, Hsu HP, Spector M, Hobbs LW. Early bone apposition in vivo on plasma-sprayed and electrochemically deposited hydroxyapatite coatings on titanium alloy. Biomaterials 2006;27:4192–203.
[17] Eliaz N, Eliyahu M. Electrochemical processes of nucleation and growth of hydroxyapatite on titanium supported by real-time electrochemical atomic force microscopy. J Biomed Mater Res A 2007;80:621–34.
[18] Eliaz N, Kopelovitch W, Burstein L, Kobayashi E, Hanawa T. Electrochemical processes of nucleation and growth of calcium phosphate on titanium supported by real-time quartz crystal microbalance measurements and X-ray photoelectron spectroscopy analysis. J Biomed Mater Res A 2009;89:270–80.
[19] Eliaz N. Electrocrystallization of calcium phosphates. Israel J Chem 2008;48:159–68.
[20] Eliaz N, Sridhar TM. Electrocrystallization of hydroxyapatite and its pH dependence. Cryst Growth Des 2008;8:3965–77.
[21] Feighan JE, Goldberg VM, Davy D, Parr JA, Stevenson S. The influence of surface-blasting on the incorporation of titanium-alloy implants in a rabbit intramedullary model. J Bone Joint Surg Am 1995;77:1380–95.

[22] Jinno T, Goldberg VM, Davy D, Stevenson S. Osseointegration of surface-blasted implants made of titanium alloy and cobalt–chromium alloy in a rabbit intramedullary model. J Biomed Mater Res. 1998;42:20–9.
[23] Hamadouche M, Witvoet J, Porcher R, Meunier A, Sedel L, Nizard R. Hydroxyapatite-coated vs. grit-blasted femoral stems: a prospective, randomized study using EBRA-FCA. J Bone Joint Surg Br 2001;83:979–87.
[24] Reikeras O, Gunderson RB. Excellent results of HA coating on a grit-blasted stem: 245 patients followed for 8–12 years. Acta Orthop Scand 2003;74:140–5.
[25] Kokubo T, Miyaji F, Kim HM. Spontaneous formation of bonelike apatite layer on chemically treated titanium metals. J Am Ceram Soc 1996;79:1127–9.
[26] Kim HM, Miyaji F, Kokubo T, Nakamura T. Effect of heat treatment on apatite-forming ability induced by alkali treatment. J Mater Sci 1997;8:342–7.
[27] Nishiguchi S, Nakamura T, Kobayashi M, Kim HM, Miyaji F, Kokubo T. The effect of heat treatment on bone-bonding ability of alkali-treated titanium. Biomaterials 1999;20:491–500.
[28] Takadama H, Kim HM, Kokubo T, Nakamura T. TEM–EDX study of the mechanism of bonelike apatite formation on bioactive titanium metal in simulated body fluid. J Biomed Mater Res 2001;57:441–8.
[29] Nishiguchi S, Fujibayashi S, Kim HM, Kokubo T, Nakamura T. Biology of alkali- and heat-treated titanium implants. J Biomed Mater Res A 2003;67:26–35.
[30] Xue W, Liu X, Zheng XB, Ding C. In vivo evaluation of plasma-sprayed titanium coating after alkali modification. Biomaterials 2005;26:3029–37.
[31] Brentel AS, de Vasconcellos LMR, Oliveira MV, Graca MLA, Vaconcellos LGO, Cairo CAA, et al. Histomophometric analysis of pure titanium implants with porous surface vs. rough surface. J Appl Oral Sci 2006;14:213–8.
[32] Peraire C, Arias JL, Bernal D, Pou J, Leon B, Arano A, et al. Biological stability and osteoconductivity in rabbit tibia of pulsed laser deposited hydroxylapatite coatings. J Biomed Mater Res A 2006;77:370–9.
[33] Hacking SA, Bobyn JD, Tanzer M, Krygier JJ. The osseous response to corundum blasted implant surfaces in a canine hip model. Clin Orthop 1999;364:240–53.
[34] Lu HB, Campbell CT, Graham DJ, Ratner BD. Surface characterization of hydroxyapatite and related calcium phosphates by XPS and TOF-SIMS. Anal Chem 2000;72:2886–94.
[35] Yang CY, Wang BC, Lee TM, Chang E, Chang GL. Intramedullary implant of plasma sprayed hydroxyapatite coating: an interface study. J Biomed Mater Res 1997;36:39–48.
[36] Stewart M, Welter JF, Goldberg VM. Effect of hydroxyapatite/tricalcium-phosphate coating on osseointegration of plasma-sprayed titanium alloy implants. J Biomed Mater Res A 2004;69:1–10.
[37] Oosterbos CJM, Vogely HCh, Nijhof MW, Fleer A, Verbout AJ, Tonino AJ, et al. Osseointegration of hydroxyapatite-coated and noncoated Ti6Al4V implants in the presence of local infection: a comparative histomorphometrical study in rabbits. J Biomed Mater Res 2002;60:339–47.
[38] Jinno T, Davy DT, Goldberg VM. Comparison of hydroxyapatite and hydroxyapatite tricalcium-phosphate coatings. J Arthroplasty 2002;17:902–9.
[39] Dorozhkin SV, Epple M. Biological and medical significance of calcium phosphates. Angew Chem Int Ed 2002;41:3130–46.
[40] Feng QL, Cui FZ, Wang H, Kim TN, Kim JO. Influence of solution conditions on deposition of calcium phosphate on titanium by NaOH-treatment. J Cryst Growth. 2000;210:735–40.
[41] Summer DR, Bryan JM, Urban RM, Kuszak JR. Measuring the volume of bone ingrowth: a comparison of three techniques. J Orthop Res 1990;8:448–52.
[42] Hacking SA, Tanzer M, Harvey EJ, Krygier JJ, Bobyn JD. Relative contributions of chemistry and topography to the osseointegration of hydroxyapatite coatings. Clin Orthop 2002;405:24–38.
[43] Schmidmaier G, Wildemann B, Schwabe P, Stange R, Hoffmann J, Südkamp NP, et al. A new electrochemically graded hydroxyapatite coating for osteosynthetic implants promotes implant osteointegration in a rat model. J Biomed Mater Res (Appl Biomater) 2002;63:168–72.
[44] Piattelli A, Trisi P. A light and laser scanning microscopy study of bone/hydroxyapatite-coated titanium implants interface: histochemical evidence of unmineralized material in humans. J Biomed Mater Res 1994;28:529–36.
[45] Park JH, Lee DY, Oh KT, Lee YK, Kim KN. Bioactive calcium phosphate coating on sodium hydroxide-pretreated titanium substrate by electrodeposition. J Am Ceram Soc 2004;87:1792–4.